Structural insight into the role of the PAS domain for signal transduction in sensor-kinase BvgS

Elian Dupré, Bernard Clantin, Youhua Yuan, Sophie Lecher, Elodie Lesne, Rudy Antoine, Vincent Villeret, Françoise Jacob-Dubuisson

Structural insight into the role of the PAS domain for signal transduction in sensor-kinase BvgS

Elian Dupré[1 *], Bernard Clantin[2], Youhua Yuan[1 *], Sophie Lecher[1], Elodie Lesne[1*], Rudy Antoine[1], Vincent Villeret[2], Françoise Jacob-Dubuisson[1 #]

[1] Univ. Lille, CNRS, Inserm, CHU Lille, Institut Pasteur de Lille, U1019-UMR 9017 – CIIL- Center for Infection and Immunity of Lille, F-59000 Lille, France

[2] U1167 - RID-AGE Univ. Lille, Inserm, CHU Lille, Institut Pasteur de Lille - CNRS ERL 9002 - Integrative Structural Biology - BP 70478 - F-59658 Villeneuve d'Ascq Cedex - France

[*] Present addresses: E Dupré, U1167 - RID-AGE Univ. Lille, Inserm, CHU Lille, Institut Pasteur de Lille - CNRS ERL 9002 - Integrative Structural Biology; E Lesne, Public Health England, Porton Down, Salisbury, United Kingdom; Y Yuan, Department of Clinical Laboratory, Henan Provincial People's Hospital, 450003 Zhengzhou, Province Henan, China

[#] Correspondence: francoise.jacob@ibl.cnrs.fr

RUNNIG TITLE: PAS domain of BvgS

KEYWORDS: Two-component system, *Bordetella pertussis*, sensor-kinases, PAS domain, virulence regulation

ABSTRACT

The two-component system BvgAS controls the virulence regulon in *Bordetella pertussis*. BvgS is the prototype of a family of sensor histidine-kinases harboring periplasmic Venus flytrap (VFT) domains. The VFT domains are connected to the cytoplasmic kinase moiety by helical linkers separated by a Per-ARNT-Sim (PAS) domain. Antagonism between the two linkers, as one forms a coiled coil when the other is dynamic and vice versa, regulates BvgS activity. Here we solved the structure of the intervening PAS domain by X-ray crystallography. Two forms were obtained that notably differ by the connections between the PAS core domain and the flanking helical linkers. Structure-guided mutagenesis indicated that those connections participate in the regulation of BvgS activity. The PAS domain thus appears to function as a switch-facilitator module whose conformation determines the output of the system. As many BvgS homologs have similar architectures, the mechanisms unveiled here are likely to generally apply to the regulation of sensor-histidine kinases of that family.

IMPORTANCE

The whooping cough agent *Bordetella pertussis* colonizes the human respiratory tract using virulence factors co-regulated by the sensory transduction system BvgAS. BvgS is a model for a family of sensor-kinase proteins, some of which are found in important bacterial pathogens. BvgS functions as a kinase or a phosphatase depending on external signals, which determines if *B. pertussis* is virulent or avirulent. Deciphering its mode of action might thus lead to new ways of fighting infections. Here we used X-ray crystallography to solve the three-dimensional structure of the domain that precedes the enzymatic moiety and identified features that regulate BvgS activity. As many sensor-kinases of the BvgS family harbor homologous domains, the mechanism unveiled here might be of general relevance.

INTRODUCTION

Signal perception and transduction are essential for adaptation to changes of environmental conditions. In eubacteria, two-component systems (TCS) are major players in the regulation of antibiotic resistance, sporulation, virulence factors expression or metabolic modifications in response to specific environmental signals (1, 2). Typically, a two-component system is composed of a sensor histidine-kinase (SHK) and a response regulator (RR) protein. Upon signal perception, the SHK autophosphorylates on a conserved His residue at the expense of ATP and transfers its phosphoryl group onto a conserved Asp residue of the RR (3, 4). Thus activated, the latter initiates specific changes enabling the cell to adapt to the new conditions. Intervening proteins or domains between the enzymatic domain of the SHK and the RR define so-called phosphorelays, thought to provide more graded responses than simple on-off switches (5). When the signal disappears, autophosphorylation and phosphotransfer cease, and the SHK dephosphorylates its RR partner, which shuts off the physiological response initiated by signal perception (6).

In *Bordetella pertussis*, the TCS BvgAS controls the expression of the virulence regulon for colonization of the human respiratory tract (7). At 37°C, in standard laboratory conditions, the SHK BvgS autophosphorylates and transfers the phosphoryl group to BvgA, which then activates transcription of the virulence genes. Low temperatures or negative modulators such as sulfate and nicotinate ions at millimolar concentrations (8) interrupt this kinase activity, shifting BvgS to a phosphatase state (9, 10). BvgS functions as a kinase by default, a feature that may be more widespread among TCSs than initially realized. The *in vivo* signals that trigger the shift to a phosphatase state remain undetermined. An intermediate mode of activity at intermediate concentrations of modulators makes BvgS a rheostat (11).

BvgS is the prototype for a large family of SHKs with extracytoplasmic Venus flytrap (VFT) domains (9). In the BvgS dimers, each monomer is composed of 2 VFT domains in

tandem, followed by an α-helical transmembrane (TM) segment that prolongs into a cytoplasm α-helical linker, called the linker 1, a PAS (Per-ARNT-Sim) domain (12), a second α-helical linker called the linker 2, a DHp (Dimerization and Histidine phosphorylation) and a CA (catalytic ATP-binding) domains that together constitute the enzymatic moiety, and finally a receiver and a HPt (Histidine-containing Phosphotransfer) domains forming a phosphorelay (Fig. 1). In the periplasm, the VFT domains form an intricate dimeric structure (9). In the cytoplasm, dimerization is mainly mediated by the two-helix linkers that can form coiled coils, and by the DHp domains (13, 14). The coiled coils are marginally stable, so that their helices can also undergo rotational dynamics, and those features are essential for activity regulation (13, 14).

The dynamics of the various domains determines the mode of activity of BvgS. In the kinase mode, the membrane-distal VFT1 domains are dynamic (9), the first linker adopts a non-canonical coiled coil conformation, and the second linker is dynamic, i.e., it does not form a coiled coil (13, 14). This is consistent with recent models of SHK mechanisms showing that kinase activity implies dynamic, asymmetric conformations of the DHp and CA domains (15-17). Binding of nicotinate to the membrane-proximal VFT2 domains rigidifies the periplasmic moiety, which induces a small vertical motion of the TM segments towards the periplasm and disrupts coiled coil formation by the linker 1 (9, 13). This causes ill-defined conformational changes that notably imply an increased distance between the PAS core domains (13) and promote coiled coil formation by the linker 2 (14). Decreased linker 2 dynamics shifts BvgS to a phosphatase state. There is thus a reciprocal relationship between the states of dynamics of the two linkers in the two modes of activity of the protein (13, 14).

PAS domains are frequent in microbial signaling proteins, where they play roles in signal perception and/or transfer (12, 18). In BvgS, the position of the PAS domain makes it an obligatory relay between the VFT and enzymatic domains. Here, we determined the X-ray

structure of a recombinant PAS domain protein. We obtained two different forms of the PAS domain monomer that notably differ by the connections of the core domain with its flanking helices. Structure-guided mutagenesis was used to identify features involved in signaling.

RESULTS

X-ray structure of PAS domain. As the recombinant protein corresponding to the PAS core domain was insoluble, we produced a larger protein encompassing significant portions of the linkers 1 and 2 of BvgS and harboring two Ala to Leu replacements in the linker 2 that enhance coiled coil formation (14, 19). Analysis of the purified protein by size exclusion chromatography indicated that it forms dimers in solution (Supplemental Figure S1A). A single crystal form was repeatedly obtained that showed a convoluted packing with 8 monomers in the asymmetric unit. The structure was solved by the multi-wavelength anomalous dispersion method and refined to a resolution of 2.4 Å, with Rwork and Rfree factors of 21.7% and 24.5%, respectively (Supplemental Table S1).

Within the asymmetric unit the eight domains adopt canonical PAS folds. Using the usual nomenclature for PAS domains (12), 5 β strands called βA, βB, βG, βH and βI form an anti-parallel β sheet in the order βB-βA-βI-βH-βG, flanked on one side by three α helices, αC, αD, and αF, encompassed in the sequence between βB and βG (Fig. 2A). One of the helices frequently found in canonical PAS domains, αE, is replaced with a loop. The PAS domain is flanked by the α helices αA' and αJ (20), which are parts of the linkers 1 and 2 and are found at the N and C termini of the PAS core domain, respectively.

The eight monomers in the asymmetric unit adopt two broadly distinct conformations, which differ by the relative orientations of the αA' and αJ helices as well as different conformations of the αC, αD, and αF segment. They are referred to hereafter as "type I" and "type II" monomers (Fig. 2B; Supplemental Figure S2). Within the asymmetric unit, PAS

126 monomers pack as two tetramers composed of two ‘central’ type I monomers (m1 and m2 in
127 the first tetramer and m5 and m6 in the second) and two ‘flanking’ type II monomers (m3 and
128 m4 in the first and m7 and m8 in the second tetramer) (Fig. 3). The two tetramers are related
129 to one another by a rotation of 130° and overall, they superimpose with a rms deviation on Cα
130 of ~0.26 Å, showing that they adopt similar conformations (Supplemental Figure S3).
131 A careful inspection of the various interfaces within and between the asymmetric units
132 indicated that the two conformations of the monomer are not induced by the crystal lattice,
133 but they are stabilized by their organization in the asymmetric unit. This suggested that the
134 two conformations may co-exist in solution, with a dimer-monomer equilibrium. However,
135 dynamic light scattering experiments with the purified protein detected particles of a single
136 size, with a hydrodynamic radius of 31.8 Å. This is compatible with the size of a dimer or a
137 tetramer, whose calculated gyration radii are both around 22 Å (21) (Supplemental Figure
138 S1B). Thus, although two forms are found in the crystal, they could not be detected in
139 solution using our experimental conditions.
140 As several PAS monomers display disordered regions, the entire polypeptide chain could
141 be fully built only for three monomers, type I monomers m1 and m6, and type II monomer
142 m7. The other two type I monomers are also well structured, with only two disordered loops,
143 between βH and βI in m2 and between αF and βG in m5 (Supplemental Figure S4). For the
144 type II monomers other than m7, the region around the αF helix and the extremities of the
145 flanking N- and C-terminal helices appear to be flexible (Supplemental Figure S4). The main
146 interface between the two tetramers within the asymmetric unit involves m6 and m7 from one
147 tetramer, and m1 and m2 from the other tetramer (Fig. 3). The packing of αF from monomer
148 m7 docked between the αJ helices of m1 and m2 stabilizes this monomer and explains why it
149 is the only type II monomer fully structured in the asymmetric unit (Fig. 3). Thus, unless

otherwise mentioned, monomers m6 and m7 will be considered in the text to refer to the type I and II conformations.

In each tetramer, the type I monomers (m1-m2 and m5-m6) are related by a two-fold symmetry axis and their interactions, which bury a surface of 750 Å², mainly involve residues of their αA' and αJ helices as well as a few contacts between their respective β sheets and αJ helices (Supplemental Table S2). The unconstrained extremities of the αA' and αJ helices diverge from one another (Fig. 3). In contrast, *in vivo* Cys scanning analyses have shown that the helices that compose the linkers cross-link with one another in a periodic manner in full-length BvgS, as expected for dimeric coiled coils (13, 14). Furthermore, the linker 2 helices are followed by the DHp domains, which typically form a 4-helix bundle in SHKs (3). Therefore the αA' and αJ helices are expected to be roughly parallel within the BvgS dimer, which is not reflected in the structure of the central dimer. Another unexpected feature is that the β sheets of the two PAS core domains are not contiguous (Supplementary Table S2). Cys scanning analyses have revealed that the PAS β sheets in full-length BvgS loosely associate in particular via two pairs of residues, His671 and Ile694 (13), whereas the residues of each pair are more than 2 nm apart in the central dimer.

The type II monomers are oriented almost perpendicular and on opposite sides of the type I monomers (Fig. 3). Although the interactions between the type I and type II monomers are non-physiological, their interfaces encompass 1000 Å² (27 to 33 residues involved between monomers m1-m4, m2-m3, m5-m8 or m6-m7) and more than 1700 Å² (42 to 47 residues involved between monomers m1-m3, m2-m4, m5-m7 or m6-m8). In the latter interfaces, the αA' helices of type II monomers are roughly packed anti-parallel to the αJ helices of type I monomers, while their αJ helices extend and pack between the αA' helix and the β-sheet core of an adjacent type I monomer. In summary, the large interfaces within and between tetramers in the asymmetric unit have enabled crystal formation by stabilizing monomer arrangements

that do not reflect their dimerization mode in BvgS, and that notably involve some non-physiological interactions between helices of neighboring monomers.

Comparison of type I and type II monomers. Among the most striking differences between the two types of monomers are the relative orientations of their N- and C-terminal helices and their connections with the PAS core domain (Fig. 2B). Thus, in type I monomers, the first residue of αJ is Ile696 of the important Asp-Ile-Thr (DIT) motif well-conserved in PAS domains (12), whereas in type II monomers the DIT motif is unfolded with the αJ helix starting only at Arg699, and therefore it is disconnected from the PAS core domain (Fig. 2; Table 1). Conversely, in type II monomers, the flanking αA' helix is closer to the PAS domain β sheet than in type I monomers (Fig. 2; Supplementary Table S3).

Other differences are found in the helical αF region and the β sheet of the PAS core domain. In the type II m7 monomer, the αF helix encompasses residues 636-650, which is longer than that in type I monomers (residues 637-645) (Fig. 2). The position of that helix is also different between the two types of monomers. As the αF helix of the m7 monomer is stabilized by adjacent helices from other monomers, the differences between the type I and type II monomers in that region are however difficult to interpret. The βH-βI loop is not well defined in most monomers, which reflects its flexibility (Supplementary Figure S4).

Recurrent principles of signaling by PAS domains have emerged from many studies (12, 22-27). In brief those studies suggest that signaling induces changes in structure and dynamics propagated by the PAS β sheet to the flanking helices, and that these changes may notably involve partial unfolding or supercoiling of the C-terminal helical extensions. We took advantage of conformational differences between the two types of monomers in those regions to explore whether they might provide clues on the mechanism of signal transduction through the BvgS PAS domain.

Importance of the connections between the PAS core domains and the αJ output helix. We first explored the connections between the PAS core domain and the N terminus of the flanking αJ helix. We have shown earlier that the Asp695 to Ala substitution in the DIT motif, a hallmark feature of PAS domains at the junction between the core domain and the N terminus of the αJ helix, abolished the kinase activity of BvgS (19). In type I monomers, Asp695 contributes to a hydrogen-bond network between the PAS core domain and the αJ helix, whereas in type II monomers the N terminus of the αJ helix is unfolded and thus disconnected from the PAS core (Fig. 4; Table 1). We disrupted other interactions by replacing Asn593, Thr697 and Arg699 with Ala, as their side chains are involved in that network in type I monomers, and we used a reporter system to determine the activity of the BvgS variants with the *lacZ* gene placed under the transcriptional control of the Bvg-regulated pertussis toxin (ptx) promoter. Strains expressing BvgS variants harboring point mutations were grown in standard conditions or in the presence of 2 mM chloronicotinate, a negative modulator of virulence. In this manner, one can determine both the levels of kinase activity of the BvgS variant relative to that of the wild type (wt) protein and its ability to respond to modulation, i.e., to shift toward a phosphatase state. In contrast, there is currently no straightforward manner to measure the phosphatase activity of BvgS.

Using the positive control strain that produces wt BvgS, we showed that 1 mM is sufficient to down-modulate activity, as already shown earlier (28) (Supplemental Figure S5). The remaining β-galactosidase (β-gal) activity comes from the non-modulated culture inoculum. The negative control strains without BvgS showed no β-gal activity (Fig. 5).

The three variants $BvgS_{N593A}$, $BvgS_{T697A}$ and $BvgS_{R699A}$ had no β-gal activity with the *ptx-lacZ* reporter, supporting the idea that the connection between αJ and the PAS core domain is necessary for kinase activity (Fig. 5A). We then used the more sensitive *PfhaB-*

225 *lacZ* reporter, as transcriptional activation of the *fhaB* promoter requires much lower amounts
226 of phosphorylated BvgA than that of the *ptx* promoter (29). Therefore, this reporter could
227 probe the residual kinase activity and the response to modulation of BvgS variants having
228 very little or no activity with the *ptx-lacZ* reporter. The three variants were also inactive with
229 the *fhaB-lacZ* reporter (Fig. 5B).
230 We have observed earlier that BvgS is readily destabilized by point mutations, and this is
231 reflected by the loss of the protein in bacteria (13). This is because its biogenesis is quite
232 complex, with both the large periplasmic and cytoplasmic moieties having to fold and to
233 dimerize in a timely manner for proper assembly. We therefore checked for the presence of
234 the inactive mutant proteins in the bacteria to determine if the corresponding mutations led to
235 biogenesis defects. In lysates of *B. pertussis*, $BvgS_{T697A}$ and $BvgS_{R699A}$ were found in low
236 amounts by immunoblot analyses using polyclonal antibodies (Supplemental Figure S6). In
237 contrast, $BvgS_{N593A}$ was not detected, arguing that the Pro592-Asn593-Pro594 motif between
238 αA' and βA is structurally critical. Altogether, the loss of kinase activity of the $BvgS_{D695A}$
239 (19), $BvgS_{T697A}$ and $BvgS_{R699A}$ variants support the idea that loosening the N terminus of αJ
240 and its connection with the PAS core domain displaces the balance of activity towards the
241 phosphatase state. The most likely reason is that the flanking αJ helices disconnected from the
242 PAS core domains are unconstrained and thus adopt a low-energy coiled coil conformation
243 that determines the phosphatase state of BvgS (14). The possibility of both kinase and
244 phosphatase activities being lost cannot be ruled out but appears to be less probable in this
245 case, as such mutations are more likely to hamper the switch between states than to abolish all
246 enzymatic activity.
247
248 **Role of the connections between the input helix and the β sheet of the PAS core domain.**
249 In type II monomers, the αA' input helix lies in the proximity of the PAS core β sheet with

hydrophobic residues Ile595 and Val597 of βA, Leu605 and Leu606 of βB, and Ile690 of βI, facing the αA' helix (Supplemental Table S3). We thus probed the importance of these β-sheet residues. We generated three BvgS variants with mild point mutations, $BvgS_{I595A}$, $BvgS_{V597A}$, and $BvgS_{L605A}$ and three variants with more drastic changes, $BvgS_{I595S + V597S}$, $BvgS_{L605S + L606S}$, and $BvgS_{I690S.}$ The $I_{595}A$ and $L_{605}A$ substitutions yielded variants with moderate kinase activity, and $BvgS_{L605A}$ remained somewhat sensitive to modulation (Fig. 5). Interestingly, $BvgS_{V597A}$ showed a higher kinase activity than wt BvgS in standard conditions. Mutations that similarly increase the kinase activity of BvgS have been reported before that are thought to displace the balance of activity toward the kinase state (30-32) (see discussion). In contrast, the drastic phenotypes of the double mutants and of $BvgS_{I690S}$ (Fig. 5) argue that the β sheet cannot be altered without severe functional consequences, as already observed (13). The first two mutant proteins were detected in the bacteria, but $BvgS_{I690S}$ was not (Supplemental Figure S6), confirming the importance of β-sheet integrity for BvgS stability and function.

Polar residues of the loop between strands βH and βI might also interact with the N-terminal part of the αA' helix, which is rich in charged residues. Notably, the βH-βI loop contains Gly residues that are likely to impart flexibility and thus to facilitate hydrogen bond formation between polar residues of βH-βI and αA'. As the structure of the full αA' helix was not resolved in the structure of type II monomers, we superposed the αA' helices of the type I m6 and type II m7 monomers to construct the N-terminal part of αA' for the latter (Supplementary Figure S7). This model supports the proximity of the βH-βI loop with the Ala573-Asn578 portion of αA' in type II monomers. We attempted to replace polar residues potentially involved in interactions between the two. However, as αA' is also involved in the linker 1 coiled coil (13), the effects of substitutions there might be difficult to interpret. Therefore, we only targeted Tyr679 and Ser682 in the βH-βI region by replacing them with

Ala. $BvgS_{Y679A}$ and $BvgS_{S682A}$ both showed low but detectable levels of kinase activity that did not respond to modulation (Fig. 5). Their phenotypes indicate that the substitutions may have disrupted interactions that stabilize the phosphatase state. Of note, a number of kinase-constitutive mutations have been reported in βH-βI (30-32) (Table 2).

Role of the PAS core for signal transduction. We also targeted other regions that differ between the two types of monomers. In type II but not in type I monomers, there are connections between the βA-βB loop and both the αD-αF loop in the helical region and the βH-βI loop in the β sheet. Lys600 and Arg603 in particular make salt bridges with Glu685 in the βH-βI loop and with Glu629 in the αD-αF loop, respectively (Table 1; Fig. 6). In type I monomers, in contrast, Arg603 makes contacts only with neighboring residues within βA-βB, and Lys600 makes no interaction (Table 1). Intriguingly, replacing Arg603 with Ala yielded two distinct, stable phenotypes, with hemolytic and non-hemolytic colonies. Such a bistable behavior of the virulence phenotype has been described before in *Bordetella* (33). The hemolytic clones showed close-to-wt levels of β-gal activity that did not respond to modulation. In contrast, the non-hemolytic ones displayed hardly any kinase activity, and $BvgS_{R603A}$ was not detected in membrane extracts of those variants, indicating a structural defect (Fig. 5; Supplemental Figure S6). Therefore, the Arg603Ala mutation yields two forms of BvgS only one of which assembles in a stable manner, further emphasizing the importance of the PAS β sheet for protein integrity. The observation that $BvgS_{R603A}$ is kinase-locked in the hemolytic variants nevertheless indicates that the kinase-phosphatase balance is affected by the mutation. We also replaced Lys600 with Ala. The $BvgS_{K600A}$ variant had detectable, low levels of activity that did not respond to modulation (Fig. 5A and B). The similar phenotypes of the two variants in that region suggest that disrupting this network of interactions favors the kinase state.

The αF helix is a full helical turn longer in type II than in type I monomers. The conformation of the αF-βG loop is maintained by a salt bridge between Glu653 and Arg657 in type II monomers only (Table 1; Figure 6), and therefore we replaced the former with Ala. This resulted in a BvgS variant with a low level of activity that seemed not to respond to modulation. Altogether, thus, substitutions in the PAS core domain reduce the kinase activity of BvgS and appear to affect the kinase/phosphatase equilibrium, suggesting that conformational changes in that region also participate in activity regulation.

DISCUSSION

BvgS is the prototype of a large family of SHKs defined by the presence of extracytoplasmic VFT domain(s). In BvgS and many homologs, the VFT and DHp domains are successively separated by a long linker 1 composed of two parallel α helices that cross the membrane and extend into the cytoplasm, a PAS domain, and a shorter helical linker 2. Regulation of BvgS activity is mediated by an antagonism between the two linkers, one forming a coiled coil when the other is dynamic and vice versa (13, 14). This work closes a gap in our model of signaling in BvgS. We propose that the PAS domain transduces changes of conformation and dynamics between the two linkers by reversibly altering its own conformation, and notably the connections between its core domain and those linkers.

We serendipitously obtained two forms of the PAS domain and took advantage of their differences to probe regions frequently involved in signaling in other PAS domains (12, 22-27). With one exception, our structure-based mutations markedly decreased BvgS activity and/or responsiveness to modulation, arguing that the PAS domain is optimized for function and that its structure and its flexibility are integral to the signaling mechanism. Nevertheless, we observed phenotypes indicative of alterations to the kinase-phosphatase balance, suggesting that the switch between states was hampered. The mutants that display β-gal

activity unresponsive to modulation are likely to be locked in kinase states, although their lower-than-wt levels of activity in non-modulated conditions indicate suboptimal conformations or dynamics. In variants with no β-gal activity, BvgS is either locked in the phosphatase state or it has lost both kinase and phosphatase activities. The former possibility is likely for mutations that disconnect the linker 2 from the PAS core domain.

We propose that a tight connection between the PAS core domain and the output αJ helix (i.e., the linker 2) exists in the kinase state, in agreement with earlier findings that this linker between the PAS and the enzymatic domains is dynamic in that state (14). Interactions between the extremity of the PAS β sheet and the αJ helix likely constrain the linker 2 and prevent it from adopting a stable coiled coil conformation. Conversely, dissociation of αJ from the core domain and local unfolding of its first helical turn favor the coiled coil formation of the linker 2. At the input side, disconnection between the PAS core domain and the αA' helix is likely to facilitate coiled coil formation by the linker 1, a feature associated with the kinase state (14). In contrast, interactions between the PAS core domain and the αA' helix impose constraints that likely prevent coiled coil formation, a situation corresponding to the phosphatase state (14). Thus, connections between the PAS core and the flanking helices most likely determine which linker can adopt a low-energy coiled coil conformation, and hence the state of activity of BvgS. According to this model, BvgS is composed of several modules, whose dynamics and conformation differ between states, and those equilibria are in thermodynamic coupling (15). In the kinase state, module 1 encompassing the VFT domains is dynamic, module 2 corresponding to the linker 1 in a coiled coil conformation is more static, and module 3 composed of the PAS core domain and the linker 2 is also dynamic. This allows the catalytic cycle that characterizes the kinase and phosphotransferase activities of SHKs (16, 17). Modulator perception shifts those equilibria toward the phosphatase state, with a VFT-domains containing module 1 more static (9), a dynamic module 2 encompassing

the linker 1 and the PAS core domain, and a more static module 3 corresponding to the linker 2 in coiled coil conformation (14). The PAS domain would thus be a switch-facilitator module that amplifies a signal by associating with one linker or the other and thereby affecting their conformation and dynamics. As BvgS works as a rheostat, intermediate states of the PAS domain can occur, as indicated by substitutions that yield intermediate levels of activity.

The PAS core domain itself appears to be involved in signal transduction, as for other PAS domains (25, 34, 35). Thus, substitutions in the βH-βI, βA-βB and αF-βG loops affect the balance of activity. However, some mutations in the β sheet appeared to destabilize BvgS. In other signaling proteins, the PAS β sheet was reported to propagate conformational or dynamic changes to an effector domain through flanking helical linkers (12, 15, 36, 37). Such a mechanical role most likely explains why structural integrity of the BvgS PAS β sheet is critical for function and stability of the protein.

Many 'constitutive' mutations in the PAS domain have been reported earlier to increase the levels of kinase activity of BvgS and/or to make it unresponsive to modulation (30-32) (Table 2). Their nature argues that they are loss-of-function mutations that displace the equilibrium toward the kinase state by disrupting interactions formed in the phosphatase state, rather than new functional features. A number of them found in the αA' helix or in the βH-βI loop likely disrupt specific interactions between the two. Other constitutive mutations remove Gly residues from, or introduce Pro residues into the βH-βI loop, which is expected to rigidify it and might hamper its capacity to interact with the αA' helix. The BvgS homolog EvgS of *Escherichia coli* can also be activated in a signal-independent manner by mutations in its PAS domain that localize to the same regions as the constitutive mutations in BvgS (38). Thus, similar signaling principles are likely to apply to other BvgS family members.

374 The PAS domain structures do not reveal a *bona fide* dimeric interface of the PAS
375 domains via their core domains. Nevertheless, using *in vivo* cross-linking analyses we have
376 shown interactions between the β sheets of the PAS domains in the BvgS dimer, with
377 negative modulation somewhat increasing their separation (13). The signaling model for
378 EvgS also involves loosening of the PAS dimeric interface (39). It is thus possible that a
379 change in the quaternary structure of the PAS domains is part of the signaling mechanism in
380 the BvgS family.
381 The Arg603Ala substitution in the βB strand yielded two distinct phenotypes that reflect
382 two conformations of BvgS. One of them has kinase activity, albeit not modulated by
383 chloronicotinate, whereas the other causes mis-assembly and degradation of the protein. PAS
384 domains are pliable, and specific point mutations may alter the register of the β sheet (40), as
385 might be the case with the substitution of Arg603. Phenotypic bistability is likely caused by
386 the positive auto-regulation of BvgS, whose gene is transactivated by phospho-BvgA in
387 standard, pro-virulence conditions. Hence, the clones in which BvgS is mi-assembled and
388 non-functional are locked in an avirulent state, in contrast to those in which BvgS is properly
389 folded.
390 In the absence of a PAS domain, as in 30% BvgS homologs, a similar regulation as in
391 BvgS can be achieved (41). The reason for the presence of a PAS domain in BvgS might thus
392 go beyond facilitating the shift between states of activity. Signal perception and mechanical
393 transmission are not mutually exclusive, and several cytoplasmic PAS domains are involved
394 in sensing, in particular of energy pathways (42, 43). We screened a library of small
395 molecules using a thermal shift assay but could not identify *bona fide* ligands of the BvgS
396 PAS domain (E. Lesne, personal communication). If it nevertheless perceives a cytoplasmic
397 signal, it is likely that binding of the ligand in the PAS cavity would affect the kinase-

phosphatase balance, with the mechanistic model of signal transduction proposed here remaining broadly valid.

MATERIALS AND METHODS

Protein production and crystallization. The construct used to produce the recombinant PAS protein is the N2C3 plasmid (19), that consists in the fragment coding for residues Ala573 to Lys720 of BvgS, harboring the $A_{709}L$ and $A_{713}L$ substitutions cloned in pASK-IBA35+. The recombinant protein includes a 6-His tag at the N terminus. It was produced from *E. coli* BL21(DE3) grown in LB medium at 37°C in a rotary shaker at 220 rpm. Expression was induced by the addition of anhydrotetracycline at 0.2 µg/mL when the optical density of the culture reached 0.3-0.4, and incubation was continued for 5 h. The cells were harvested by centrifugation, and the cell pellets were resuspended in 20 mM imidazole pH 6.5 (binding buffer) containing 5 µg/ml of DNase I and EDTA-free protease inhibitor cocktail (Roche). Bacteria were broken by repeated passages in a French pressure cell, and the cell debris were removed by centrifugation for 20 min at 10,000 g. The supernatant was loaded onto a Ni^{2+}-Sepharose metal-chelate column equilibrated with the binding buffer. After washing steps with 50 mM imidazole (pH 6.5), the protein was eluted with 500 mM imidazole (pH 6.5). Concentrated fractions between 15 and 30 mg/ml were obtained after elution and dialyzed against the binding buffer. Crystallization screening was carried out using the PHClear Suite, the AmSO4 Suite and the Cryos Suite (Qiagen) and Clear Strategy Screen I and II (Molecular Dimensions). Optimal crystallization conditions were obtained in sodium acetate 0.1 M (pH 5), 2% PEG 6000. Crystals were evaluated at synchrotron beamlines (ESRF and SOLEIL). Only one crystal form was obtained, that belonged to space group $P2_12_12$, with cell parameters suggesting that the asymmetric unit could contain from 6 to 12 monomers, as estimated from the Matthews coefficient. Most crystals diffracted to

resolutions between 3 and 4Å. We observed that soaking crystals with Eu-DO3A sometimes resulted in an improved high-resolution limit. Crystals were thus soaked for 10-30 seconds in the same medium containing 15% glycerol and 100 mM Eu-DO3A (Lanthanide Phasing Kit, Jena Bioscience) before vitrification.

Structure determination. Attempts to solve the structure by the molecular replacement method using the various PAS domain structures available in the PDB failed, probably due to the lack of significant sequence homology with the BvgS PAS, to the high number of PAS domains contained within the asymmetric unit, and to the distinct structural conformations adopted by the protein in the crystal, which were revealed when the structure was finally determined. In order to solve the structure experimentally by the MAD technique, we measured diffraction data of the crystals soaked in a solution containing 100 mM Eu-DO3A at wavelengths corresponding to the peak and inflexion points of Europium, as well as at a remote wavelength. Data were collected at the ID23-2 and ID19 beamlines at the ESRF and processed using XDS (44). Phasing was done using SHARP (45), and model building was accomplished in PHENIX (46), using a combination of automatic building as well as extensive manual reconstruction in COOT (47). In order to improve the high-resolution diffraction limit, a large number of crystals were subsequently screened, allowing us to measure a dataset at a resolution of 2.3Å. This dataset was further used to finalize model building as well as to refine the structure to 2.3Å resolution with PHENIX. Statistics for this dataset and datasets used for the MAD phasing are reported in Supplemental Table S1. Refinement statistics obtained in PHENIX are also reported. Final Rfree is 24.5%, with a good stereochemistry for the model.

The final model comprises eight PAS domains in the asymmetric unit, organized in two similar tetramers composed of chains A, B, C, D and E, F, G, H (corresponding to monomers

448 m1-m4 and m5-m8, respectively). In each tetramer, two monomers are related by a two-fold
449 symmetry axis (m1-m2 and m5-m6) and flanked on opposite sides by two individual adjacent
450 monomers (m3, m4 and m7, m8). In flanking monomers 3, 4 and 8, the region between helix
451 αC and strand βG (~residues 60 to 95 comprising helices αD and αF), which covers one face
452 of the five-stranded β sheet of the PAS domains, is highly dynamic and poorly defined in the
453 electron density map. The last flanking monomer 7 is fully defined, probably because in this
454 case this region is stabilized at the interface between the two tetramers. The coordinates as
455 well as diffraction amplitudes have been deposited in the PDB under accession code 6ZJ8.
456
457 **Structure analysis**. The structure interfaces and assemblies were assessed using
458 PDBePISA (https://www.ebi.ac.uk/pdbe/pisa/). Hydrogen bond networks and structural
459 illustrations were processed using the PyMOL Molecular Graphics System, Version 1.8.2.3,
460 Schrödinger, LLC.
461
462 **Gel filtration and Dynamic Light Scattering.** A S75 (16/600) Superdex column was
463 equilibrated in 50 mM imidazole (pH 6.8). A solution of the recombinant PAS protein at 6.4
464 mg/mL was injected, and the chromatography was performed at 0.5 mL/min. Dynamic light
465 scattering measurements were performed in triplicate on a Zetasizer Nano-S (Malvern), using
466 a 1.5 mg/mL protein solution in 20 mM Tris-HCl (pH 6.8), 50 mM NaCl and a two-fold
467 dilution of the same solution.
468
469 **Strains, plasmids, and culture conditions.** *B. pertussis* was first grown on Bordet-
470 Gengou blood agar plates for 2 days at 37°C and then cultured in modified SS medium at
471 37°C under rotary shaking at 220 rpm. All the BvgS variants were constructed by site-
472 directed mutagenesis using the QuikChange II Site-Directed Mutagenesis Kit (Agilent

technologies) on a recombinant pUC19 plasmid harboring a 780-bp SacI-XbaI fragment that encompasses the sequences coding for the linker 1, the PAS domain, the linker 2 and the first portion of the DHp domain of BvgS (9). The *bvgS* sequence used here is that with a Glu codon at position 705 as in most *B. pertussis* strains, rather than the Lys codon found in *Tohama I* (48). After sequencing, the fragment was ligated in pUCmpla (9) in replacement of the wt fragment. The 4.7-kb of the latter plasmid was introduced into pBBR1-MCS4, a low-copy, mobilizable plasmid that replicates in *Bordetella*. The pBBRmpla variants were introduced by conjugation into $BPSM_{new\Delta AS}$ (9) carrying chromosomal *ptx-lacZ* or *fhaB-lacZ* transcriptional fusions.

Measurement of BvgS activity. Recombinant *B. pertussis* strains were grown in modified SS medium supplemented or not with 2 mM chloronicotinate. The cultures were stopped at mid-exponential phase, harvested by centrifugation, resuspended to an OD_{600} of 5 and broken using a Hybaid Ribolyser apparatus for 50 sec at speed 6 in tubes containing silica spheres (MP biomedicals, lysing B matrix). β-galactosidase activities were measured as described (49) on at least 3 different clones using three technical replicates, and the means and standard deviations were calculated. The positive and negative control strains were $BPSM_{new\Delta AS}$ complemented with a wt version of the pBBRmpla plasmid and with the empty vector, respectively. Of note, as negative modulators slow down the growth of *B. pertussis* when BvgS is expressed from a plasmid as was the case here, cultures need to be started with large inocula from non-modulated precultures. This is the reason why the positive control strain retained some β-gal activity after overnight growth in modulating conditions. The remaining activity observed is because this very stable enzyme is carried over from the preculture.

Detection of inactive BvgS variants. The recombinant bacteria were cultured as above and resuspended in 50 mM TrisHCl (pH 7), 150 mM NaCl supplemented with protease inhibitors. They were lysed by passages in a French pressure cell, and the membrane proteins were harvested by ultracentrifugation from the clarified lysates. The samples were analyzed by denaturing gel electrophoresis using 4-8% gels, followed by immunoblotting with anti-BvgS antibodies (19).

ACKNOWLEDGMENTS

We thank Hugo Bidois for the first mutations and β gal analyses. This work was initiated with the grant ANR-13-BSV8-0002-01 to FJD and then pursued with the financial support of Inserm and the University of Lille. Y. Yuan acknowledges the financial support from the Henan Provincial Hospital. The funders had no role in designing the experiments or analyzing the data.

REFERENCES

1. Cheung J, Hendrickson WA. 2010. Sensor domains of two-component regulatory systems. Curr Opin Microbiol 13:116-23.
2. Krell T, Lacal J, Busch A, Silva-Jimenez H, Guazzaroni ME, Ramos JL. 2010. Bacterial sensor-kinases: diversity in the recognition of environmental signals. Annu Rev Microbiol 64:539-559.
3. Jacob-Dubuisson F, Mechaly A, Betton JM, Antoine R. 2018. Structural insights into the signalling mechanisms of two-component systems. Nat Rev Microbiol 16:585-593.
4. Zschiedrich CP, Keidel V, Szurmant H. 2016. Molecular Mechanisms of Two-Component Signal Transduction. J Mol Biol 428:3752-75.
5. Gao R, Stock AM. 2009. Biological insights from structures of two-component proteins. Annu Rev Microbiol 63:133-54.
6. Gao R, Stock AM. 2013. Probing kinase and phosphatase activities of two-component systems in vivo with concentration-dependent phosphorylation profiling. Proc Natl Acad Sci U S A 110:672-7.
7. Melvin JA, Scheller EV, Miller JF, Cotter PA. 2014. *Bordetella pertussis* pathogenesis: current and future challenges. Nat Rev Microbiol 12:274-88.
8. Melton AR, Weiss AA. 1993. Characterization of environmental regulators of *Bordetella pertussis*. Infect Immun 61:807-15.
9. Dupre E, Herrou J, Lensink MF, Wintjens R, Vagin A, Lebedev A, Crosson S, Villeret V, Locht C, Antoine R, Jacob-Dubuisson F. 2015. Virulence Regulation with Venus Flytrap

Domains: Structure and Function of the Periplasmic Moiety of the Sensor-Kinase BvgS. PLoS Pathog 11:e1004700.
10. Uhl MA, Miller JF. 1996. Central role of the BvgS receiver as a phosphorylated intermediate in a complex two-component phosphorelay. J Biol Chem 271:33176-80.
11. Deora R, Bootsma HJ, Miller JF, Cotter PA. 2001. Diversity in the *Bordetella* virulence regulon: transcriptional control of a Bvg-intermediate phase gene. Mol Microbiol 40:669-83.
12. Möglich A, Ayers RA, Moffat K. 2009. Structure and signaling mechanism of Per-ARNT-Sim domains. Structure 17:1282-94.
13. Lesne E, Dupre E, Locht C, Antoine R, Jacob-Dubuisson F. 2017. Conformational changes of inter-domain linker mediate mechanical signal transmission in sensor-kinase BvgS. J Bacteriol 199:e00114-17.
14. Lesne E, Krammer EM, Dupre E, Locht C, Lensink MF, Antoine R, Jacob-Dubuisson F. 2016. Balance between Coiled-Coil Stability and Dynamics Regulates Activity of BvgS Sensor Kinase in *Bordetella*. MBio 7:e02089.
15. Bhate MP, Molnar KS, Goulian M, DeGrado WF. 2015. Signal transduction in histidine kinases: insights from new structures. Structure 23:981-94.
16. Casino P, Miguel-Romero L, Marina A. 2014. Visualizing autophosphorylation in histidine kinases. Nat Commun 5:3258.
17. Mechaly AE, Sassoon N, Betton JM, Alzari PM. 2014. Segmental helical motions and dynamical asymmetry modulate histidine kinase autophosphorylation. PLoS Biol 12:e1001776.
18. Henry JT, Crosson S. 2011. Ligand-binding PAS domains in a genomic, cellular, and structural context. Annu Rev Microbiol 65:261-86.
19. Dupre E, Wohlkonig A, Herrou J, Locht C, Jacob-Dubuisson F, Antoine R. 2013. Characterization of the PAS domain in the sensor-kinase BvgS: mechanical role in signal transmission. BMC Microbiol 13:172.
20. Diensthuber RP, Bommer M, Gleichmann T, Moglich A. 2013. Full-length structure of a sensor histidine kinase pinpoints coaxial coiled coils as signal transducers and modulators. Structure 21:1127-36.
21. Wilkins DK, Grimshaw SB, Receveur V, Dobson CM, Jones JA, Smith LJ. 1999. Hydrodynamic radii of native and denatured proteins measured by pulse field gradient NMR techniques. Biochemistry 38:16424-31.
22. Ayers RA, Moffat K. 2008. Changes in quaternary structure in the signaling mechanisms of PAS domains. Biochemistry 47:12078-86.
23. Berntsson O, Diensthuber RP, Panman MR, Bjorling A, Gustavsson E, Hoernke M, Hughes AJ, Henry L, Niebling S, Takala H, Ihalainen JA, Newby G, Kerruth S, Heberle J, Liebi M, Menzel A, Henning R, Kosheleva I, Moglich A, Westenhoff S. 2017. Sequential conformational transitions and alpha-helical supercoiling regulate a sensor histidine kinase. Nat Commun 8:284.
24. Key J, Hefti M, Purcell EB, Moffat K. 2007. Structure of the redox sensor domain of Azotobacter vinelandii NifL at atomic resolution: signaling, dimerization, and mechanism. Biochemistry 46:3614-23.
25. Little R, Salinas P, Slavny P, Clarke TA, Dixon R. 2011. Substitutions in the redox-sensing PAS domain of the NifL regulatory protein define an inter-subunit pathway for redox signal transmission. Mol Microbiol 82:222-35.
26. Monzel C, Degreif-Dunnwald P, Gropper C, Griesinger C, Unden G. 2013. The cytoplasmic PASC domain of the sensor kinase DcuS of *Escherichia coli*: role in signal transduction, dimer formation, and DctA interaction. Microbiologyopen 2:912-27.

27. Slavny P, Little R, Salinas P, Clarke TA, Dixon R. 2010. Quaternary structure changes in a second Per-Arnt-Sim domain mediate intramolecular redox signal relay in the NifL regulatory protein. Mol Microbiol 75:61-75.
28. Dupre E, Lesne E, Guerin J, Lensink MF, Verger A, de Ruyck J, Brysbaert G, Vezin H, Locht C, Antoine R, Jacob-Dubuisson F. 2015. Signal Transduction by BvgS Sensor-Kinase: Binding of Modulator Nicotinate Affects Conformation and Dynamics of Entire Periplasmic Moiety. J Biol Chem 290:23307-319.
29. Jones AM, Boucher PE, Williams CL, Stibitz S, Cotter PA. 2005. Role of BvgA phosphorylation and DNA binding affinity in control of Bvg-mediated phenotypic phase transition in *Bordetella pertussis*. Mol Microbiol 58:700-13.
30. Goyard S, Bellalou J, Mireau H, Ullmann A. 1994. Mutations in the *Bordetella pertussis bvgS* gene that confer altered expression of the *fhaB* gene in *Escherichia coli*. J Bacteriol 176:5163-6.
31. Manetti R, Arico B, Rappuoli R, Scarlato V. 1994. Mutations in the linker region of BvgS abolish response to environmental signals for the regulation of the virulence factors in *Bordetella pertussis*. Gene 150:123-7.
32. Miller JF, Johnson SA, Black WJ, Beattie DT, Mekalanos JJ, Falkow S. 1992. Constitutive sensory transduction mutations in the *Bordetella pertussis bvgS* gene. J Bacteriol 174:970-9.
33. Mason E, Henderson MW, Scheller EV, Byrd MS, Cotter PA. 2013. Evidence for phenotypic bistability resulting from transcriptional interference of bvgAS in *Bordetella bronchiseptica*. Mol Microbiol 90:716-33.
34. Gong W, Hao B, Mansy SS, Gonzalez G, Gilles-Gonzalez MA, Chan MK. 1998. Structure of a biological oxygen sensor: a new mechanism for heme-driven signal transduction. Proc Natl Acad Sci U S A 95:15177-82.
35. Key J, Moffat K. 2005. Crystal structures of deoxy and CO-bound bjFixLH reveal details of ligand recognition and signaling. Biochemistry 44:4627-35.
36. Garcia D, Watts KJ, Johnson MS, Taylor BL. 2016. Delineating PAS-HAMP interaction surfaces and signalling-associated changes in the aerotaxis receptor Aer. Mol Microbiol 100:156-72.
37. Wang C, Sang J, Wang J, Su M, Downey JS, Wu Q, Wang S, Cai Y, Xu X, Wu J, Senadheera DB, Cvitkovitch DG, Chen L, Goodman SD, Han A. 2013. Mechanistic insights revealed by the crystal structure of a histidine kinase with signal transducer and sensor domains. PLoS Biol 11:e1001493.
38. Johnson MD, Bell J, Clarke K, Chandler R, Pathak P, Xia Y, Marshall RL, Weinstock GM, Loman NJ, Winn PJ, Lund PA. 2014. Characterization of mutations in the PAS domain of the EvgS sensor kinase selected by laboratory evolution for acid resistance in *Escherichia coli*. Mol Microbiol 93:911-27.
39. Sen H, Aggarwal N, Ishionwu C, Hussain N, Parmar C, Jamshad M, Bavro VN, Lund PA. 2017. Structural and Functional Analysis of the *Escherichia coli* Acid-Sensing Histidine Kinase EvgS. J Bacteriol 199.
40. Evans MR, Card PB, Gardner KH. 2009. ARNT PAS-B has a fragile native state structure with an alternative beta-sheet register nearby in sequence space. Proc Natl Acad Sci U S A 106:2617-22.
41. Lesne E, Dupré E, Lensink MF, Locht C, Antoine R, Jacob-Dubuisson F. 2018. Coiled-coil antagonism regulates activity of Venus flytrap-domain-containing sensor-kinases of the BvgS family. mBIO 9:e02052-17.
42. Sobran MA, Cotter PA. 2019. The BvgS PAS Domain, an Independent Sensory Perception Module in the B*ordetella bronchiseptica* BvgAS Phosphorelay. J Bacteriol 201.

43. Taylor BL, Zhulin IB. 1999. PAS domains: internal sensors of oxygen, redox potential, and light. Microbiol Mol Biol Rev 63:479-506.
44. Kabsch W. 2010. XDS. Acta Cryst D 66:125-132.
45. Bricogne G, Vonrhein C, Flensburg C, Schiltz M, Paciorek W. 2003. Generation, representation and flow of phase information in structure determination: recent developments in and around SHARP 2.0. Acta Cryst D 59:2023-2030.
46. Liebschner D, Afonine PV, Baker ML, Bunkóczi G, Chen VB, Croll TI, Hintze B, Hung LW, Jain S, McCoy AJ, Moriarty NW, Oeffner RD, Poon BK, Prisant MG, Read RJ, Richardson JS, Richardson DC, Sammito MD, Sobolev OV, Stockwell DH, Terwilliger TC, Urzhumtsev AG, Videau LL, Williams CJ, Adams PD. 2019. Macromolecular structure determination using X-rays, neutrons and electrons: recent developments in Phenix. Acta Cryst D 75:861-877
47. Emsley P, Lohkamp B, Scott WG, Cowtan K. 2010. Features and development of Coot. Acta Crystallogr D Biol Crystallogr 66:486-501.
48. Herrou J, Debrie AS, Willery E, Renaud-Mongenie G, Locht C, Mooi F, Jacob-Dubuisson F, Antoine R. 2009. Molecular evolution of the two-component system BvgAS involved in virulence regulation in Bordetella. PLoS One 4:e6996.
49. Antoine R, Alonso S, Raze D, Coutte L, Lesjean S, Willery E, Locht C, Jacob-Dubuisson F. 2000. New virulence-activated and virulence-repressed genes identified by systematic gene inactivation and generation of transcriptional fusions in *Bordetella pertussis*. J Bacteriol 182:5902-5905.

Table 1. Intra-monomer hydrogen bonds and other potential interactions between the side chains of the residues of interest and side-chain or main-chain (N^{mc}, O^{mc}) atoms of other residues.

Residue	Sec. Struct.	Interacting atoms and distances (Å)			
		Monom 6 (Type I)		**Monom 7 (Type II)**	
N593	αA'-βA loop	δO-η^2N R699 (αJ):	2.9		
N593				-	
I595*	βA	-		*	
V597*	βA	-		*	
K600	βA-βB loop	-			
K600				ζN-ε^1O E685 (βH-βI):	3
K600				ζN-O^{mc} L686 (βH-βI):	3.3
R603	βB	εN-δ^2O D599 (βA) :	3		
R603		η^2N-δ^2O D599 (βA) :	3.1		
R603		η^2N-ε^2O E601 (βA-βB):	3.2		
R603				η^1N-O^{mc} G624 (αD-αF):	3.3
R603				η^1N-ε^1O E629 (αD-αF):	2.9
R603				η^2N-ε^2O E629 (αD-αF):	3.4
R603				εN-ε^1O E601 (βA-βB):	3.5
L605*	βB	-		*	
L606*	βB	-		*	
E653	αF-βG loop	-			
E653				ε^1O-η^1N R657 (βG):	2.7
Y679$^{\$}$	βH	-		$	
S682$^{\$}$	βH-βI loop	-		$	
I690*	βI	-		*	
D695	βI	δ^1O-N^{mc} T697 (αJ):	3		
D695		δ^1O-N^{mc} E698 (αJ):	3.1		
D695				δ^2O-η^1N R670 (βH):	2.8
T697	αJ	γO-N^{mc} H671 (βH):	2.8		
T697	βI-αJ loop			-	
R699	αJ	η^1N-N^{mc} D695 (βI-αJ):	2.8		
R699		η^2N-δO N593 (αA'-βA):	2.9		

* denote hydrophobic residues of the PAS core β sheet oriented towards the αA' helix in type and possibly in van der Waals contacts with it in type II monomers, that were targeted in this study (see also Supplemental Table S3). $ denotes residues of the PAS core domain potentially involved in interactions with αA' in type II monomers (see text and Supplemental Table S3). Note that a distance of 3.2 Å is considered the upper limit for hydrogen bond formation, but we chose to also show slightly longer distances given the resolution of the structure.

Table 2. Constitutive mutations in BvgS.

Residue	Substitution(s)	Position in structure	References
Arg570	Ala, Leu, His	αA' (a in coiled coil)	(13, 29, 30)
Arg575	Cys	αA'	(30)
Leu577	Cys	αA' (a/d in coiled coil)	(13)
Asp579	Cys	αA'	(13)
Gln580	Arg, Ser	αA' (d in coiled coil)	(29, 30)
Phe583	Cys	αA'	(13)
Leu587	Cys	αA'	(13)
Ile595	Cys	αA'	(13)
Leu606	Cys	βB	(13)
Cys607	Ala	βB	(19)
His643	Ala	αF	(19)
Leu647	Pro	αF / αF-βG loop	(28)
Thr648	Lys	αF / αF-βG loop	(28)
Thr676	Cys	βH	(13)
Tyr679	Cys	βH-βI loop	(28)
Gly680	Ser	βH-βI loop	(29)
Leu686	Pro	βH-βI loop	(28)
Gly688	Ser	βI	(30)
Ile689	Cys	βI	(13)

The 'a' and 'd' positions represent interfacial residues of a two-parallel-helix coiled coil, i.e., residues that are in close proximity with a residue of the other helix and that determine coiled coil stability. The Leu647 and Thr648 residues are part of the αF helix and of the αF-βG loop in type II and type I monomers, respectively.

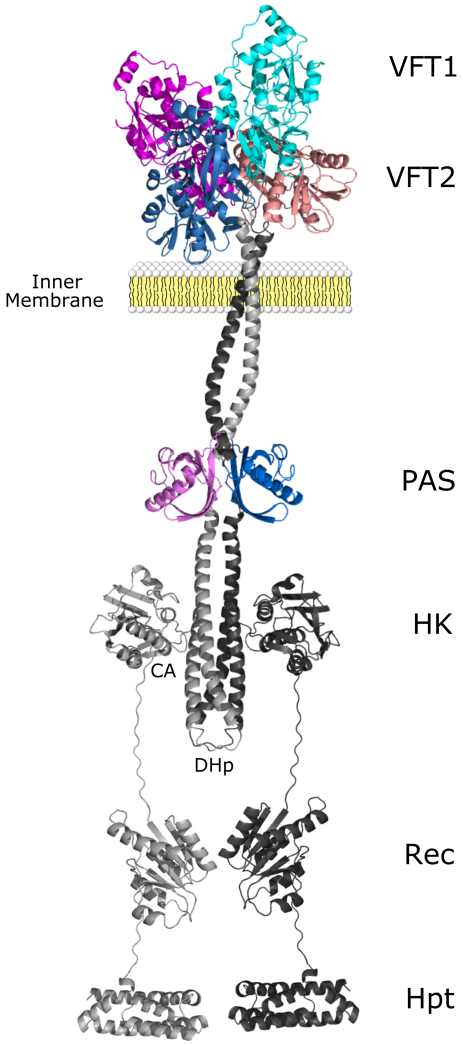

Figure 1. Model representation of the full-length BvgS dimer based on original structures and models. One monomer is represented in shades of blue and dark gray for original structures and structural models, respectively, and the other is in shades of pink and light gray. VFT structure: pdb accession number 4Q0C; PAS structure: this work, pdb 6ZJ8; HK: modeled from pdb 4GCZ; Rec: modeled from pdb 2AYX, and Hpt: modeled from pdb 1BDJ. The linkers flanking the PAS domain were modeled, since their orientations in the structures obtained here are not compatible with the organization of full-length BvgS.

708

709

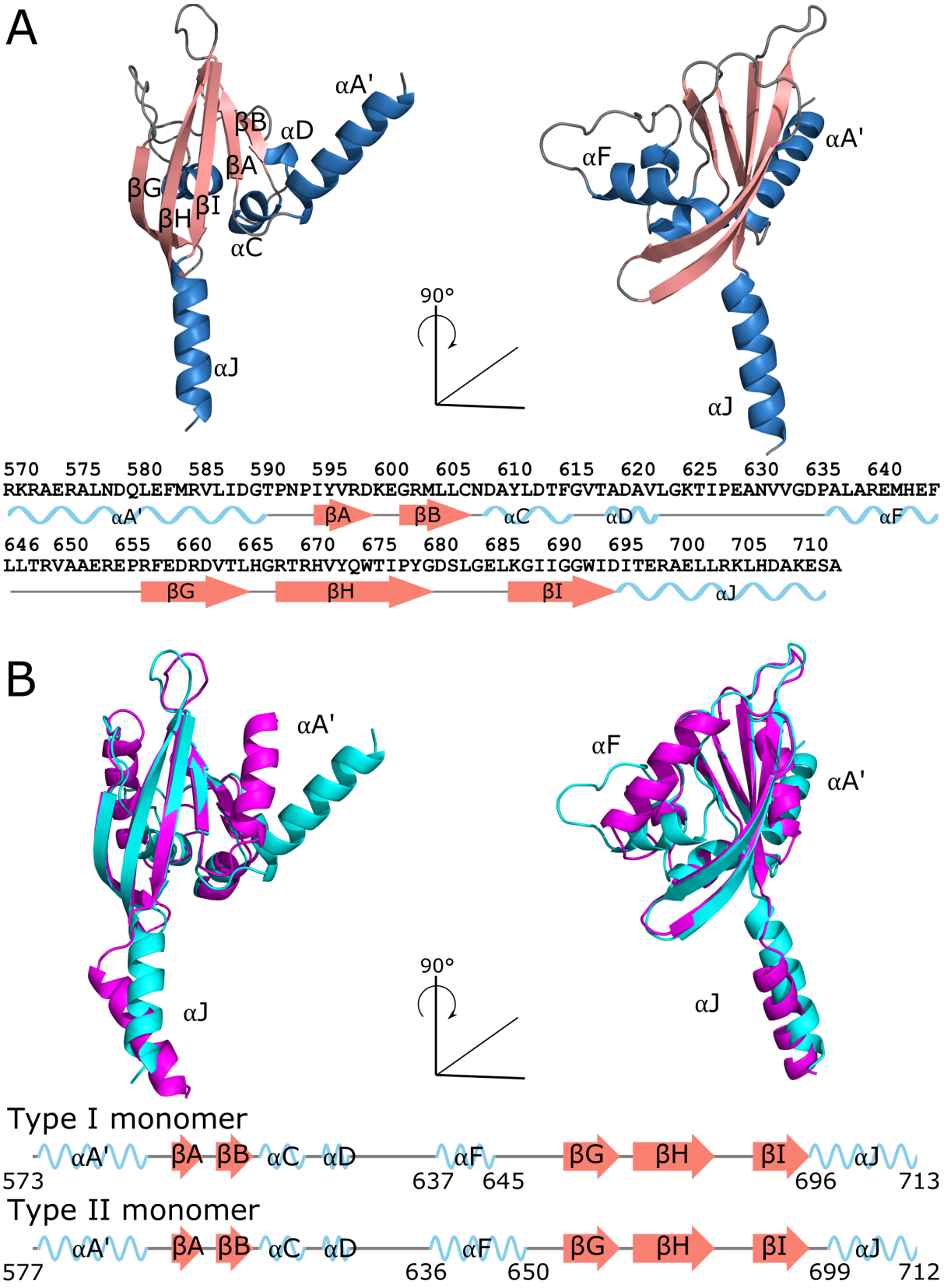

Figure 2. Cartoon representation of the BvgS PAS domain. (A) Type I monomer (m6) represented with α helices in blue and β strands in pink. All secondary structures are labeled

except helix αF which, in the left panel, is located behind the β sheet and for clarity is thus labeled only in the right panel. The sequence of the PAS domain is indicated below, with the corresponding secondary structure elements of type I monomers. The grey lines represent loops. (B) Structural alignment of a type I monomer in blue (m6) and a type II monomer in pink (m7). The secondary structure plots of m6 and m7 below show slight differences in architecture between type I and type II monomers.

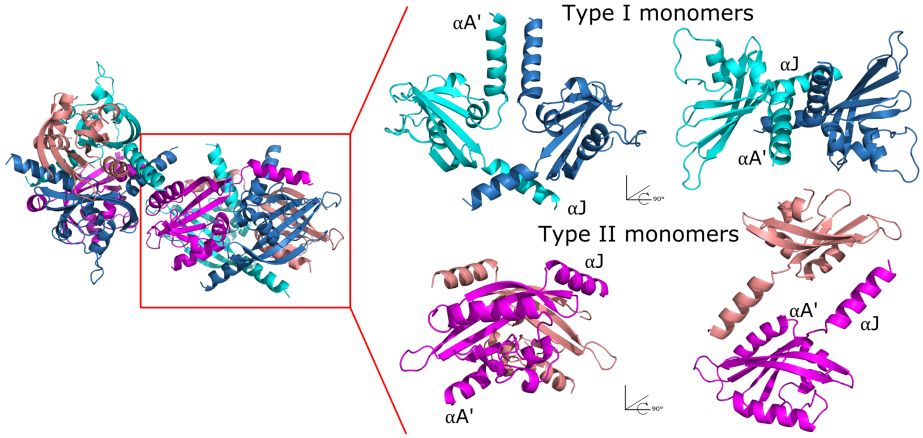

Figure 3. Cartoon representation of the molecular packing of BvgS PAS domains in the crystal. Type I and type II monomers are represented in shades of blue and pink, respectively. The asymmetric unit comprises eight monomers packed into two similar tetramers, each with two type I monomers and two type II monomers. Within the tetramer type I monomers pack as a dimer and are related by a two-fold symmetry axis. They are flanked on opposite sides by two type II monomers. The two tetramers are not related by a typical crystallographic symmetry operation.

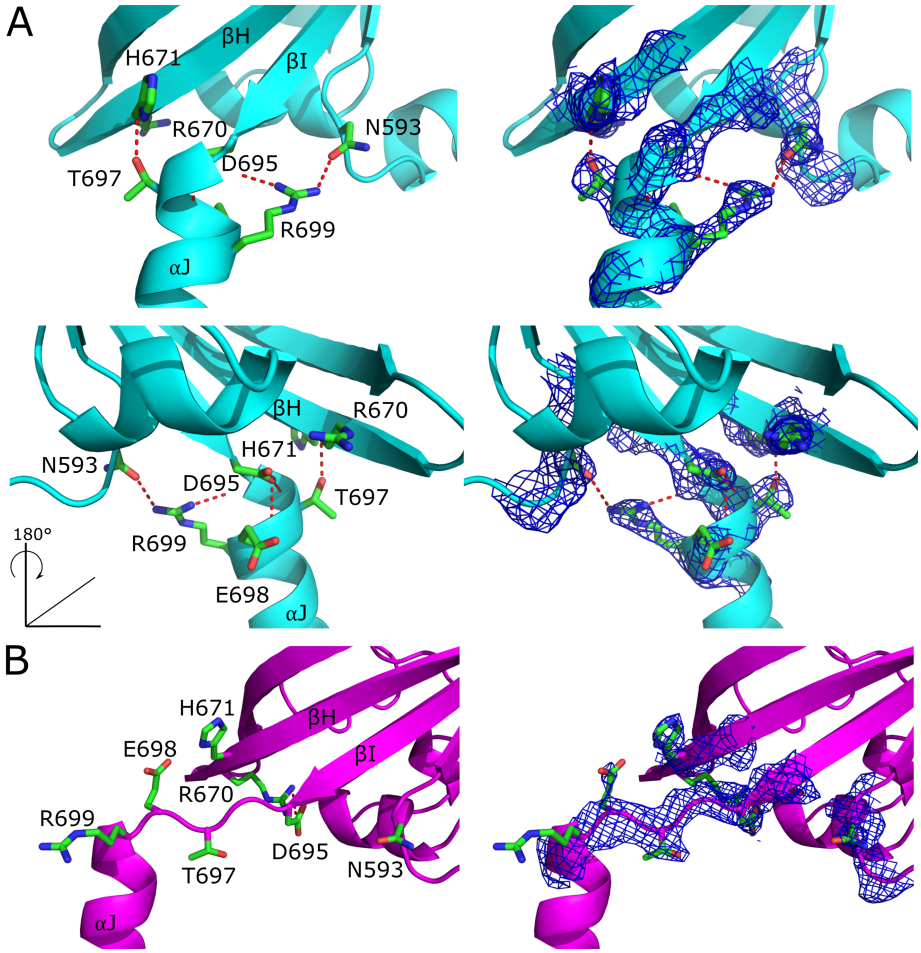

Figure 4. Interaction network around the conserved "DIT" motif in type I monomers (A) and type II monomers (B) in cartoon and stick representation. The right panels show electron densities in that region. Hydrogen bonds are represented with red dashed lines.

722 **Figure 4.**

723

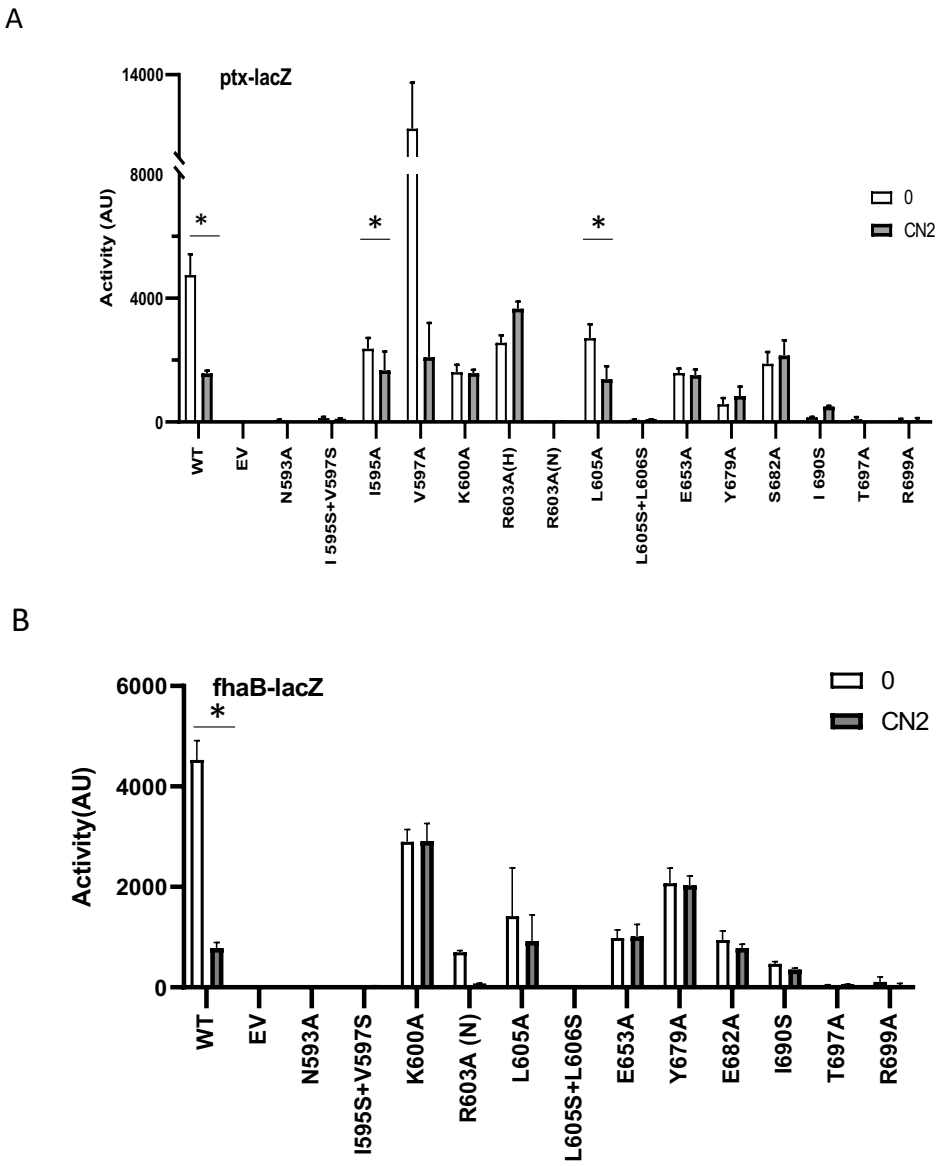

Figure 5. Effect of the substitutions in the PAS domain and its flanking helices on BvgS activity. (A) A *ptx-lacZ* transcriptional fusion was used to determine the activities of the BvgS variants under standard conditions (0) or after the addition of 2 mM chloronicotinate to the culture medium (CN2) compared to those of wild type BvgS (WT) and of the strain with an empty vector (EV). The BvgS variants are indicated by the substitution that they harbor. For the $BvgS_{R603A}$ variant, hemolytic (H) and non-hemolytic (N) clones were analyzed. (B) A *fhaB-lacZ* transcriptional fusion was used as above for the variants that showed no or very little activity with *ptx-lacZ*. The values are given in arbitrary units, with the means and

standard deviations. *, statistically significant difference using the non-parametric two-tailed Mann-Whitney test (confidence 95%).

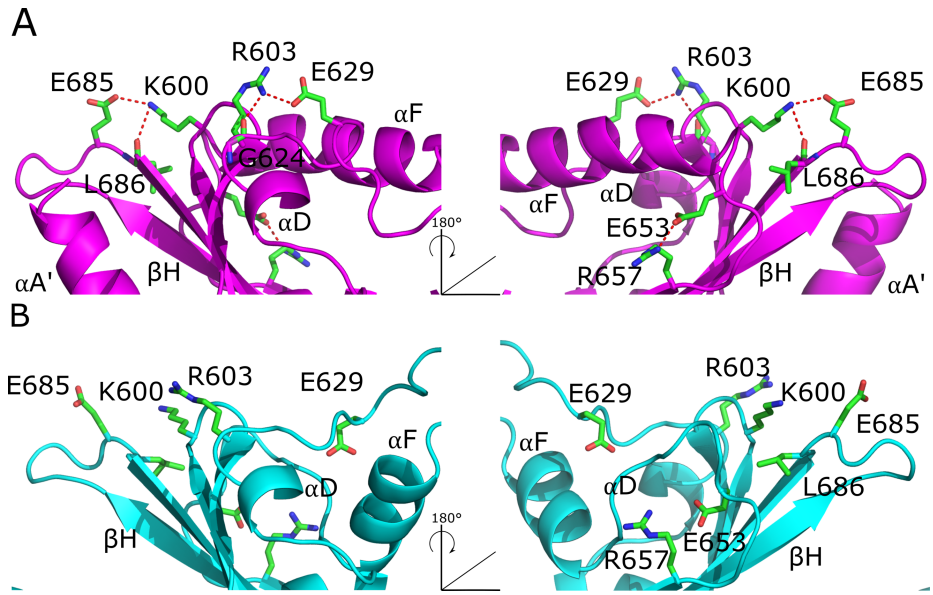

Figure 6. Interaction network in the PAS core domain shown in cartoon and sticks representation. The same color code was used as in Fig. 4, with type II monomers depicted in pink (A) and type I monomers in blue (B). Hydrogen bonds between side chains are indicated with dashed red lines.

Figure 6.